

Measurements of the $^{27}\text{Al}(\alpha, n)$ Thick Target Yield Near Threshold

K. Brandenburg,^a G. Hamad,^a Z. Meisel,^{*,a} C. R. Brune,^a D. E. Carter,^a J. Derkin,^a D. C. Ingram,^a Y. Jones-Alberty,^a B. Kenady,^a T. N. Massey,^a M. Saxena,^a D. Soltész,^a S. K. Subedi,^a and J. Warren^a

^a*Institute of Nuclear & Particle Physics
Department of Physics & Astronomy
Ohio University, Athens, Ohio 45701, USA*

*Email: meisel@ohio.edu

Number of pages: 14

Number of tables: 0

Number of figures: 2

Abstract

We present results from direct measurements of the $^{27}\text{Al}(\alpha, n)$ thick target yield from laboratory energies $E_\alpha \approx 3\text{--}5$ MeV, performed with the HeBGB neutron detector at the Edwards Accelerator Laboratory. Our measurements have a small energy cadence in order to address discrepancies and sparseness of thick-target yield data sets existing for this energy region. We find general agreement with existing data sets, including yields derived from cross section data, while resolving a discrepancy between existing thick-target yield data sets for $E_\alpha \approx 4 - 5$ MeV. However, for $E_\alpha < 3.5$ MeV, our results are substantially lower than previous thick-target yield data and somewhat larger than yields calculated from existing cross section data. Our data complete the energy-range needed for estimates of the $^{27}\text{Al}(\alpha, n)$ contribution to neutrino and dark matter detector backgrounds and result in increased viability of $^{27}\text{Al}(\alpha, n)$ as a tool for fusion plasma diagnostics, e.g. at the National Ignition Facility.

Keywords — thick-target yield, neutron background, NIF diagnostic

I. INTRODUCTION

$^{27}\text{Al}(\alpha, n)$ is a significant neutron source from transuranic waste material [1], could potentially be used for high energy density plasma diagnostics at the National Ignition Facility (NIF) or the International Thermonuclear Experimental Reactor (ITER) [2], is a potential source of neutrons from some molten salt reactor components [3], contributes to dark matter detector backgrounds [4], and plays a role in shock-driven nucleosynthesis in core collapse supernovae [5, 6]. As such, it is important to have a precise characterization this reaction. For nuclear applications, the thick-target yield is of particular importance, as α -particles emitted from α -decaying nuclides will generally fully stop within nearby components.

Five cross section data sets exist for the $^{27}\text{Al}(\alpha, n)$ cross section for α beam energies $E_\alpha < 7 \text{ MeV}$ [7, 5, 8, 9], though the data of Ref. [7] have a strong contribution from background. The data sets of Refs. [7, 9] and one set from Ref. [8] have a small energy spacing that enables variations in the cross section to be observed. Two of the data sets in this energy range come from ^{27}Al targets of moderate thickness [5, 8], resulting in a smoother excitation function. In principle, each of these can be converted to thick-target yields by integrating the ratio of the cross section and stopping power. However, there are discrepancies between Ref. [8] and [9]. Ref. [9] attribute this to carbon contamination issues of Ref. [8]. As such, there is a large difference in the yield depending on the adopted cross section data set [10]. Additionally, there is an uncertainty contribution due to the adopted stopping-power. For instance, when Ref. [11] calculated thick-target yields from the cross section data of Refs. [5, 8], they required an arbitrary normalization to agree with the directly measured thick-target yields of Ref. [12].

To date, two thick-target yield data sets exist for $^{27}\text{Al}(\alpha, n)$ [12, 13]. Ref. [12] employed a neutron counter, while Ref. [13] performed their measurements using the activation technique. The data sets are in agreement for $E_\alpha > 5 \text{ MeV}$, though the data set of Ref. [13] has rather sparse energy spacing over the entire energy range of interest, while the data set of Ref. [12] has a single point for $E_\alpha < 4 \text{ MeV}$ (to be compared to the $^{27}\text{Al}(\alpha, n)$ reaction threshold of 3.034 MeV). The discrepancy between the two data sets can result in different estimates for neutron backgrounds resulting from α -decaying nuclides in environments with fissile materials or actinide contaminants. The presence of only two data points with $E_\alpha < 3.5 \text{ MeV}$ for Ref. [13], and none for Ref. [12], hinders the use of $^{27}\text{Al}(\alpha, n)$ as a potential diagnostic reaction for fusion plasmas, e.g. at NIF [2].

To remedy these issues, we performed measurements of $^{27}\text{Al}(\alpha, n)$ thick-target yields with a small energy cadence for $E_\alpha < 5$ MeV using the HeBGB neutron counter [14] at the Edwards Accelerator Laboratory at Ohio University [15]. In Section II we describe our measurement approach. We discuss the results in Section III and provide concluding remarks in Section IV.

II. MEASUREMENT DETAILS

Measurements were performed at the Edwards Accelerator Laboratory at Ohio University [15]. The full set-up is described in detail in Ref. [14], though we cover the most relevant details here. A helium beam produced by an Alphatross ion source was accelerated using a 4.5 MV T-Type tandem pelletron to an energy between 3-5 MeV, departing the accelerator as ^{++}He . The beam was analyzed with an energy-calibrated 90° dipole magnet and slits with a gap of 0.254 cm, resulting in a beam energy uncertainty of 0.36%. The beam passed through a 0.5 cm diameter gold-plated collimator located approximately 48 cm upstream of the target location and was impinged on a thick ^{27}Al target located on a gold-plated ladder at the center of the HeBGB moderator. Typical beam intensities on-target were ~ 50 nA.

The ^{27}Al thick-target was made of Reynolds Wrap aluminum foil, cleaned by an alcohol solution, and folded-over several times to make a stopping target. Reynolds Wrap is manufactured to have high-purity of aluminum, where possible contaminants are <1% by weight of magnesium, silicon, titanium, chromium, iron, manganese, copper, and zinc, and < 0.15% of all other elements [17, 18]. We confirmed this purity using Rutherford backscattering (RBS) and particle-induced X-ray emission (PIXE) ion beam analysis, using the set-up described in Refs. [15, 19]. Results from RBS and PIXE measurements performed with a 2.2 MeV α beam are shown in Fig. 1. RBS results only show evidence for aluminum and iron, where calculations performed with RUMP [16] identified an iron abundance <1% and confirmed that the abundance of the aforementioned suspected contaminants is $\ll 1\%$. The deviation between the simulated and measured RBS spectra at low channel number (energy) is due to the absence of multiple-scattering effects in the RUMP calculations [20]. The PIXE spectrum in Fig. 1 confirms that the target is primarily aluminum with some iron contamination and minor contributions from other elements. For context, a comparison is provided to Puratronic high-purity (99.99% pure metals-basis) aluminum foil.

For isotopes of the iron contamination identified in our target in Fig. 1, the (α, n) thresholds

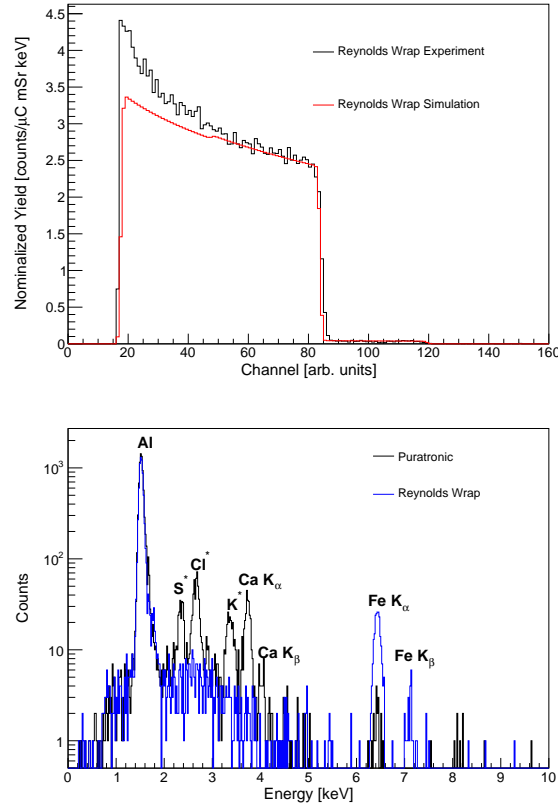


Fig. 1. Results from ion beam analysis of the aluminum target used in this work. The upper panel compares results of RBS measurements to calculations performed with RUMP [16], where the main feature is due to aluminum and the small plateau from channels $\sim 90 - 120$ is due to iron. The lower panel compares the results of PIXE measurements for our target material (Reynolds Wrap) to high-purity aluminum foil (Puratronic), where X-rays from elements present in the foils are identified.

are 1.457 MeV (^{57}Fe), 3.833 MeV (^{58}Fe), 5.468 MeV (^{56}Fe), and 6.255 MeV (^{54}Fe). However, the Coulomb barrier suppresses (α, n) cross sections for these isotopes far below $^{27}\text{Al}(\alpha, n)$ at the same E_α . Consequently, thick-target yields for natural iron are around two-orders of magnitude (or more) lower than the thick-target yields from ^{27}Al [12]. Additionally, we performed measurements of the neutron yield in HeBGB for E_α below the $^{27}\text{Al}(\alpha, n)$ threshold and found yields on the order of the background (0.24 ± 0.05 n/s for empty-target runs near $E_\alpha = 3$ MeV). This provides further evidence that target contamination did not provide significant contributions to our measured $^{27}\text{Al}(\alpha, n)$ thick-target yields for most energies. For energies just above threshold, the beam-on-target yields measured just below threshold were used to estimate the background

contribution.

For our thick-target yield measurements, the incident charge was measured by summing the beam current of the target ladder and target chamber within HeBGB. To ensure the entirety of the beam was on-target, at each measurement energy the beam was first tuned through an empty space in the target ladder and the beam intensity I_α was recorded on a downstream Faraday cup. Empty target measurements were periodically recorded for enough time to provide high-statistics background measurements. The number of detected neutrons $N_{n,\text{det}}$ was counted using the ^3He and BF_3 neutron-sensitive proportional counters, configured as described in Ref. [14]. A pulser, adjusted to provide a signal outside of the neutron spectrum, was used to monitor the proportional counter dead-time and therefore the live fraction f_{live} of the data acquisition.

While HeBGB provides nearly 4π coverage, our MCNP [21] simulation results show some dependence of the neutron detection efficiency ϵ on the neutron angular distribution [14]. However, given the high excitation energy populated within the ^{31}P compound nucleus by $^{27}\text{Al} + \alpha$, a number of levels are likely to participate in the reaction and thus significantly anisotropic angular distributions are not anticipated. This is consistent with existing angular distribution data for this reaction [22]. We therefore assume an isotropic angular distribution for our neutron detection efficiency.

The yield at each energy is calculated by $Y = N_{n,\text{det}}/(I_\alpha t \epsilon f_{\text{live}})$, where $I_\alpha t$ is the integrated charge on the target for a measurement and $\epsilon = 7.5 \pm 1.2\%$. Our neutron detection efficiency dominates our yield uncertainty, with the exception of yields within a few-hundred keV of the reaction threshold, where the background uncertainty is significant. The integrated charge contributes a 1% uncertainty. We add all uncertainties in quadrature to obtain our total yield uncertainty.

III. RESULTS AND DISCUSSION

We present our thick-target yield measurement results^a in the upper-panel of Fig. 2 (also), where we compare to thick-target yield measurement data of Ref. [12, 13] and the evaluation results of Ref. [11], who integrated the cross section data of Refs. [5, 8] with the stopping power of Ref. [23] and scaled the results to match Ref. [12]. We also compare to thick-target yields calculated using thin-target cross section data of Ref. [9] and the stopping power of Ref. [23], where we include a 5%

^aSee the Supplemental Material for a table of our measured yield.

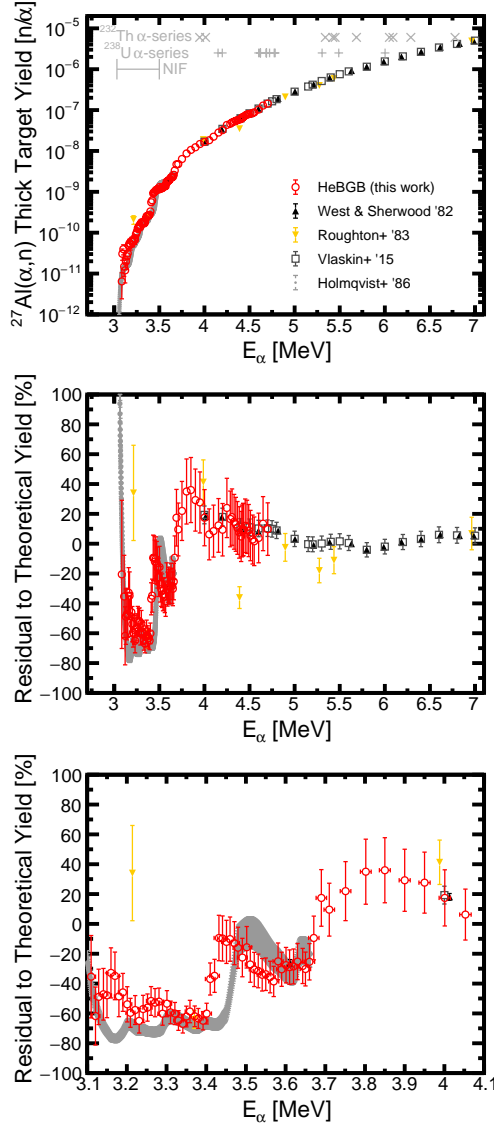


Fig. 2. The upper panel shows $^{27}\text{Al}(\alpha, n)$ thick-target yields measured in this work (HeBGB), compared to yield measurements of Refs. [12] (West & Sherwood '82) and [13] (Roughton+ '83), the evaluated thick-target yield of Ref. [11] (Vlaskin+ '15), and the thick-target yield resulting from integrating the cross-section data of Ref. [9] with stopping powers from Ref. [23]. The ^{232}Th and ^{238}U decay series E_α with decay branches greater than 1% are also shown by the \times and $+$, respectively, while a bracket $|-|$ indicates the energy range for α -particles relevant for plasma fusion diagnostics (NIF). The middle panel shows a residual between the upper-panel results and theoretical yields calculated using the `Talysv1.8` [24] default cross section and `SRIM2013` [23] stopping power, where the theoretical yields are arbitrarily scaled by a factor of 0.8. The lower panel is the same as the middle panel, but focusing on a narrower energy range.

uncertainty in the stopping power based on the world data for helium stopping in aluminum at these energies [25]. For context, the upper panel of Fig. 2 highlights E_α of typical actinide contaminants in neutrino and dark matter detectors [26], as well as the E_α range relevant for fusion plasma diagnostics [2]. In order to compare these thick-target yields in more detail, the middle and lower panels of Fig. 2 shows the residual to an arbitrary theoretical yield. We calculated the $^{27}\text{Al}(\alpha, n)$ cross section using default settings of `Talysv1.8` [24], determined the stopping power using the stopping power from `SRIM2013` [23], and adjusted the resulting thick-target yield by an arbitrary normalization of $\times 0.8$ in order to approximately go through the average trend of the data sets.

Our $^{27}\text{Al}(\alpha, n)$ thick-target yields are overall in good agreement with existing data sets, where we agree with Ref. [12] rather than Ref. [13] at the energies where these two data sets disagree. Just above the reaction threshold, our results show slightly larger yields than yields calculated with the cross section data of Ref. [9], while being substantially lower than the lowest-energy thick-target yield data point of Ref. [13]. The discrepancy near threshold is likely explained by background subtraction issues. Ref. [9] performed background measurements for various E_α impinged on a gold backing and on their aluminum target while below threshold. It is possible that the background for the measurements performed with the gold backing was not the same as the background for the aluminum thick-target yield measurements. This could be due to different rates of carbon build-up, e.g. due to different quality of vacuum or different a beam tune impinging on more or less carbon-coated components upstream of the target location, or different room background rates due to changing environment conditions [27]. For the results reported here, our target ladder system, including an empty frame for background measurements, enabled us to obtain frequent background measurements for the same E_α , same beam tune, and same setup at almost the same time as the thick-target yield measurements.

Meanwhile, we also disagree with yields derived from Ref. [9] cross sections as to the location of the step-like yield increase in the $E_\alpha = 3.4 - 3.5$ energy range. While yields resulting from Ref. [9] have a step-like increase (from a resonance-like feature in the cross section) at $E_\alpha = 3.5$ MeV, we find that the increase occurs roughly 50 keV lower. This is likely due to the fact that Ref. [9] actually measured thick-target yields, which they did not report, but rather differentiated to arrive their reported cross sections. Small uncertainties in the beam energy, as well as insufficiently fine energy spacing between measurement points, can compound to shift the energy of features in the

resulting thick-target yield. Shifts could also occur due to adopting different stopping powers, but these uncertainties (discussed above) are included in the uncertainty band.

Our results demonstrate that the $^{27}\text{Al}(\alpha, n)$ thick-target yields of Ref. [12] are preferred over the results of Ref. [13]. We complement the former data set, by extending $^{27}\text{Al}(\alpha, n)$ thick-target yield data down to 60 keV above the reaction threshold. Our data complete the energy-range needed for estimates of the $^{27}\text{Al}(\alpha, n)$ contribution to neutrino and dark matter detector backgrounds. Meanwhile, our results modify the $^{27}\text{Al}(\alpha, n)$ yield that would be estimated for a fusion plasma diagnostic scenario, e.g. at NIF, relative to estimates based on prior thick-target data or thick-target yields calculated from existing cross section data. Specifically, our results imply larger yields from $^{27}\text{Al}(\alpha, n)$, and therefore higher-precision constraints on the mix of ablator material in the the DT fuel [2]. Detailed calculations are highly complex, e.g. see Ref. [28] for calculations of $^{10}\text{B}(\alpha, n)$ yields at NIF, and are well beyond the scope of the present work.

IV. CONCLUSION

We performed thick-target yield measurements of $^{27}\text{Al}(\alpha, n)$ for $E_\alpha = 3 - 5$ using the HeBGB neutron counter at the Edwards Accelerator Laboratory at Ohio University. Our results remedy the sparseness in thick-target yield data for $E_\alpha < 5$ MeV and resolve the discrepancy between prior results of Ref. [12] and [13]. Our directly measured thick-target yields are slightly larger than thick-target yields inferred from the cross section data of Ref. [9], who provide the only high-energy resolution cross section data near threshold, while being substantially lower than the only thick-target yield data reported in this energy range [13]. Meanwhile, we find that the step-like increase in the yield near $E_\alpha \sim 3.5$ MeV occurs \sim 50 keV lower in energy relative to prior results [9]. Our data complete the energy-range needed for estimates of the $^{27}\text{Al}(\alpha, n)$ contribution to neutrino and dark matter detector backgrounds and result in increased viability of $^{27}\text{Al}(\alpha, n)$ as a tool for fusion plasma diagnostics.

ACKNOWLEDGMENTS

This work was supported in part by the U.S. Department of Energy Office of Science under Grants No. DE-FG02-88ER40387 and DE-SC0019042 and the U.S. National Nuclear Security Administration through Grants No. DE-NA0003883 and DE-NA0003909. The helium ion source was provided by Grant No. PHY-1827893 from the U.S. National Science Foundation. We also benefited from support by the U.S. National Science Foundation under Grant No. PHY-1430152 (Joint Institute for Nuclear Astrophysics – Center for the Evolution of the Elements).

DISCLOSURE STATEMENT

The authors report there are no competing interests to declare.

DATA AVAILABILITY STATEMENT

Thick target yields reported in this work are available as a text file in the Supplemental Material.

REFERENCES

- [1] R. GEHRKE, J. BAKER, J. HARTWELL, C. RIDDE, and C. MCGRATH, “Measurement of neutron-to- γ ray production ratios from (α, n) reactions for their application to assay TRU waste,” *Nucl. Instrum. Meth. A*, **511**, 3, 444 (2003); [https://doi.org/10.1016/S0168-9002\(03\)02011-4](https://doi.org/10.1016/S0168-9002(03)02011-4).
- [2] C. J. CERJAN ET AL., “Dynamic high energy density plasma environments at the National Ignition Facility for nuclear science research,” *J. Phys. G.*, **45**, 3, 033003 (2018) URL <http://stacks.iop.org/0954-3899/45/i=3/a=033003>.
- [3] F.-Y. OUYANG, C.-H. CHANG, B.-C. YOU, T.-K. YEH, and J.-J. KAI, “Effect of moisture on corrosion of Ni-based alloys in molten alkali fluoride FLiNaK salt environments,” *J. Nucl. Mater.*, **437**, 1, 201 (2013); <https://doi.org/10.1016/j.jnucmat.2013.02.021>.
- [4] D.-M. MEI, C. ZHANG, and A. HIME, “Evaluation of (α, n) induced neutrons as a background for dark matter experiments,” *Nucl. Instrum. Meth. A*, **606**, 3, 651 (2009); <https://doi.org/10.1016/j.nima.2009.04.032>, URL <http://www.sciencedirect.com/science/article/pii/S016890020900833X>.
- [5] A. J. HOWARD, H. B. JENSEN, M. RIOS, W. A. FOWLER, and B. A. ZIMMERMAN, “Measurement and Theoretical Analysis of Some Reaction Rates of Interest in Silicon Burning,” *Astrophys. J.*, **188**, 131 (1974); [10.1086/152694](https://doi.org/10.1086/152694).
- [6] S. K. SUBEDI, Z. MEISEL, and G. MERZ, “Sensitivity of ^{44}Ti and ^{56}Ni Production in Core-collapse Supernova Shock-driven Nucleosynthesis to Nuclear Reaction Rate Variations,” *Astrophys. J.*, **898**, 1, 5 (2020); [10.3847/1538-4357/ab9745](https://doi.org/10.3847/1538-4357/ab9745).
- [7] R. M. WILLIAMSON, T. KATMAN, and B. S. BURTON, “ F^{19} , Na^{23} , and $\text{Al}^{27}(\alpha, n)$ Reactions,” *Phys. Rev.*, **117**, 1325 (1960); [10.1103/PhysRev.117.1325](https://doi.org/10.1103/PhysRev.117.1325), URL <https://link.aps.org/doi/10.1103/PhysRev.117.1325>.
- [8] D. S. FLYNN, K. K. SEKHARAN, B. A. HILLER, H. LAUMER, J. L. WEIL, and F. GABARD, “Cross sections and reaction rates for $^{23}\text{Na}(p, n)^{23}\text{Mg}$, $^{27}\text{Al}(p, n)^{27}\text{Si}$, $^{27}\text{Al}(\alpha, n)^{30}\text{P}$, $^{29}\text{Si}(\alpha, n)^{32}\text{S}$, and $^{30}\text{Si}(\alpha, n)^{33}\text{S}$,” *Phys. Rev. C*, **18**, 1566 (1978); [10.1103/PhysRevC.18.1566](https://doi.org/10.1103/PhysRevC.18.1566).

[9] B. HOLMQVIST and E. RAMSTRÖM, “The Excitation Function of the $^{27}\text{Al}(\alpha, \text{n})^{30}\text{P}$ Reaction and its Astrophysical Application,” *Phys. Scripta*, **33**, 2, 107 (1986); 10.1088/0031-8949/33/2/003.

[10] S. S. WESTERDALE, A. JUNGHANS, R. J. DEBOER, M. PIGNI, and P. DIMITRIOU, “(α, n) Nuclear Data Evaluations and Data Needs Summary Report of the Technical Meeting 8–12 November 2021 (virtual event),” , INDC International Nuclear Data Committee, INDC(NDS)-0836, Vienna, Austria (2022)URL <https://www-nds.iaea.org/publications/indc/indc-nds-0836.pdf>.

[11] G. VLASKIN, Y. KHOMYAKOV, and V. BULANENKO, “Neutron Yield of the Reaction (α, n) on Thick Targets Comprised of Light Elements,” *Atom. Energy*, **117**, 357 (2015).

[12] D. WEST and A. SHERWOOD, “Measurements of thick-target (α, n) yields from light elements,” *Ann. Nucl. Energy*, **9**, 11, 551 (1982); 10.1016/0306-4549(82)90001-9.

[13] N. ROUGHTON, T. INTRATOR, R. PETERSON, C. ZAIDINS, and C. J. HANSEN, “Thick-target measurements and astrophysical thermonuclear reaction rates: Alpha-induced reactions,” *Atom. Data Nucl. Data*, **28**, 2, 341 (1983); [https://doi.org/10.1016/0092-640X\(83\)90021-9](https://doi.org/10.1016/0092-640X(83)90021-9).

[14] K. BRANDENBURG ET AL., “The ^3He BF_3 Giant Barrel (HeBGB) Neutron Detector,” *J. Instrum.*, **17** (2022); 10.1088/1748-0221/17/05/P05004., P05004, (2022).

[15] Z. MEISEL, C. BRUNE, S. GRIMES, D. INGRAM, T. MASSEY, and A. VOINOV, “The Edwards Accelerator Laboratory at Ohio University,” *Physcs. Proc.*, **90**, 448 (2017); <https://doi.org/10.1016/j.phpro.2017.09.050>.

[16] L. R. DOOLITTLE, “Algorithms for the rapid simulation of Rutherford backscattering spectra,” *Nucl. Instrum. Meth. B*, **9**, 3, 344 (1985); 10.1016/0168-583X(85)90762-1.

[17] B. R. WARD, S. A. LEVY, and G. A. SLOAN, “Method for making aluminum foil and cast strip stock for aluminum foilmaking and products therefrom,” (1995)URL <https://patents.google.com/patent/US5466312>, U.S. Patent No. US5466312A.

[18] B. R. WARD, R. E. HUGHES, and J. P. MARTIN, “Method for making aluminum alloy foil and products therefrom,” (1998)URL <https://patents.google.com/patent/US5725695>, U.S. Patent No. US5725695A.

[19] D. C. INGRAM, W. M. JADWISIENCZAK, F. EHRÉ, C. LABBÉ, and F. GOURBILLEAU, “RBS Analysis of Down-conversion Layers Comprising Two Rare-Earth Elements,” *Physcs. Proc.*, **90**, 32 (2017); 10.1016/j.phpro.2017.09.015.

[20] P. BAUER, E. STEINBAUER, and J. P. BIERSACK, “Rutherford backscattering beyond the single scattering model,” *Nucl. Instrum. Meth. B*, **79**, 1-4, 443 (1993); 10.1016/0168-583X(93)95383-G.

[21] T. GOORLEY ET AL., “Initial MCNP6 Release Overview,” *Nucl. Technol.*, **180**, 3, 298 (2012); 10.13182/NT11-135.

[22] R. BATCHELOR and J. H. TOWLE, “Neutron Spectra and Differential Cross Sections of the Reactions $^{19}\text{F}(\alpha, n)^{22}\text{Na}$ and $^{27}\text{Al}(\alpha, n)^{30}\text{P}$,” *P. Phys. Soc.*, **73**, 2, 307 (1959); 10.1088/0370-1328/73/2/420., URL <https://doi.org/10.1088/0370-1328/73/2/420>.

[23] J. F. ZIEGLER, M. D. ZIEGLER, and J. P. BIERSACK, “SRIM - The stopping and range of ions in matter (2010),” *Nucl. Instrum. Meth. B*, **268**, 11-12, 1818 (2010); 10.1016/j.nimb.2010.02.091.

[24] A.J. Koning, S. Hilaire and M.C. Duijvestijn, “TALYS-1.0”, Proceedings of the International Conference on Nuclear Data for Science and Technology - ND2007, April 22-27, 2007, Nice, France, eds. O. Bersillon, F. Gunsing, E. Bauge, R. Jacqmin and S. Leray, EDP Sciences, 2008, p. 211-214.

[25] C. MONTANARI and P. DIMITRIOU, “The IAEA stopping power database, following the trends in stopping power of ions in matter,” *Nucl. Instrum. Meth. B*, **408**, 50 (2017); [https://doi.org/10.1016/j.nimb.2017.03.138.](https://doi.org/10.1016/j.nimb.2017.03.138), URL <https://www.sciencedirect.com/science/article/pii/S0168583X1730397X>.

[26] A. GANDO ET AL., “Constraints on θ_{13} from a three-flavor oscillation analysis of reactor antineutrinos at KamLAND,” *Phys. Rev. D*, **83**, 052002 (2011); 10.1103/PhysRevD.83.052002.

[27] S. WALSH, M. MILLETT, and M. NELSON, “A Spatial and Temporal Characterization of the Background Neutron Environment at the Navy and Marine Corps Memorial Stadium,” *Journal of Radiation Effects: Research and Engineering*, **35**, 170 (2017)URL <https://apps.dtic.mil/sti/citations/AD1044825>.

[28] D. LONARDONI ET AL., “First measurement of the ${}^{10}\text{B} (\alpha, n) {}^{13}\text{N}$ reaction in an inertial confinement fusion implosion at the National Ignition Facility: Initial steps toward the development of a radiochemistry mix diagnostic,” *Phys. Plasmas*, **29**, 5, 052709 (2022); 10.1063/5.0079676.